Effects of different typed unsymmetrical squaraines on their material properties and Coulomb interactions in organic photovoltaic devices[†]

Lin Yang,[†a,b] Daobin Yang,[†a,c] Yao Chen,[a] Jianglin Wu,[a] Zhiyun Lu,[a] Hisahiro Sasabe,[c] Junji Kido,[c] Takeshi Sano,[c] and Yan Huang*[a]

[a] Key Laboratory of Green Chemistry and Technology (Ministry of Education), College of Chemistry, Sichuan University, Chengdu 610064, P. R. China.

[b] Department of Medicinal Chemistry, School of Pharmacy, Southwest Medical University, Luzhou, Sichuan 646000, P. R. China.

[c] Department of Organic Materials Science, Research Center for Organic Electronics (ROEL), Frontier Center for Organic Materials (FROM), Yamagata University, Yonezawa, 992-8510, Japan.

[†]These authors contributed equally.

Table of Contents

Experimental Section

1.1. General

NMR spectra were recorded on a Bruker Avance AV II-400 MHz instrument with tetramethylsilane as internal standard. High resolution mass spectra were measured on a Shimadzu LCMS-IT-TOF. FT-IR spectra were recorded on a Perkin-Elmer 2000 infrared spectrometer with KBr pellets under ambient atmosphere. The purity of these three USQs is measured by PerkinElmer Flaxer LC. Absorption spectra of the target compounds in 3×10^{-6} mol L^{-1} chloroform solution and thin film states were measured with a Perkin Elmer Lamdba 950 UV-Vis scanning spectrophotometer. The thin film was fabricated by spin-casting the USQ chloroform solution with a concentration of 5 mg mL^{-1} (1500 rpm, 35 s) on quartz substrates.

1.2. Electrochemistry measurement

Cyclic voltammetry was performed in 0.10 mol L^{-1} tetrabutylammonium perchlorate/anhydrous dichloromethane (2.5×10^{-4} mol L^{-1}) with a LK 2010 electrochemical work station, using a three-electrode cell with a Pt disk working electrode, a Pt wire counter electrode and a $Ag/AgNO_3$ (0.1 mol L^{-1} in acetonitrile) reference electrode. Solutions were pre-degassed by argon bubbling for 30 min prior to each experiment. At the end of each measurement, ferrocenium/ferrocene redox couple was added as an internal potential reference. The highest occupied molecular orbital (HOMO) energy levels of these three USQs compounds were determined from the peak of the oxidation waves by comparison with the Fc/Fc^+ redox couple whose energy level is 4.80 eV below vacuum,[1, 2, 3] HOMO and LUMO energy levels were deduced from the following equations:

$$\text{HOMO} = (-4.8 - qE_{ox}) \text{ eV} \qquad (1)$$

$$\text{LUMO} = (-4.8 - qE_{red}) \text{ eV} \qquad (2)$$

1.3. X-ray single crystallography

The crystallographic data for **BIISQ** is obtained from the literature (CCDC 981604)[4] and the other two USQs reported here have been deposited in the Cambridge Database (CCDC 1487657 for **TIISQ**, and 1487656 for **IDPSQ**). Single crystal samples of **TIISQ** and **IDPSQ** were obtained from dichloromethane/cyclohexane, and dichloromethane/hexane, respectively. Single crystal X-ray diffraction data were obtained on a Xcalibur E X-ray single crystal diffractometer equipped with graphite monochromator Cu-Kα (λ= 1.5418 Å) or Mo-Kα (λ= 0.7107 Å) radiation. The data collection was executed using CrysAlisPro program. The structures were determined using direct method and successive Fourier difference syntheses (SHELXS-97) and refined using full-matrix least-squares procedure on F2 with anisotropic thermal parameters for all non-hydrogen atoms (SHELXL-97). Additional refinement details and the resulting factors for these three USQs are given in **Table S1**.

1.4. Electrostatic potential (ESP) calculation

The geometry optimizations for the ground states of the USQs were performed by density functional theory (DFT) at the B3LYP/6-31G level based on their crystal structures using Gaussian 09 software.[5] The ESP maps of the USQs were calculated with an isovalue of the electron density set to 0.001 e/bohr^3 by Multiwfn software[6, 7] and drew by visual molecular dynamics (VMD) software.

1.5. Device fabrication and characteristics

Photovoltaic devices were fabricated on indium-tin oxide (ITO) coated-glass substrate (sheet resistance = 15 Ω sq^{-1}) with a layered structure of ITO/MoO$_3$ (8 nm)/USQ:PC$_{71}$BM (1:3, wt%, 60 nm)/C$_{70}$ (0 or 4 nm)/BCP (6, 10, 14 or 18 nm)/Al (100 nm). The patterned ITO-coated glass substrates were cleaned through sequential sonication in detergent, deionized water, acetone and isopropanol for 20 min each. The cleaned substrates were dried in an oven at 65°C for 12 h before using. The substrate was treated by UV-ozone for 30 min, then immediately transferred into a high vacuum chamber for deposition of 8 nm MoO$_3$ at pressure of less than 1×10^{-4} Pa with a rate of 0.2 Å s^{-1}. Subsequently, the photoactive layer (thickness: 60 ± 5 nm) was fabricated by spin-casting a blend of the USQ and PC$_{71}$BM in chloroform solution with a total concentration of 20 mg mL^{-1} (3500 rpm, 45 s) under a N$_2$-filling glove box at 25°C. Finally, the substrates were transferred back to the high-vacuum chamber, where C$_{70}$, BCP and Al were deposited as the top electrode at pressures of less than 2×10^{-4} Pa with a rate of 0.20 Å s^{-1}, 0.20 Å s^{-1} and 2.0~3.0 Å s^{-1}, respectively. The active area of OPV cells is 9 mm^2. To obtain the average data related to device performance, several batches of devices (4 cells per batch) for each set of conditions were fabricated and tested. Current density-voltage (*J-V*) and external quantum efficiency (EQE) characterization of organic photovoltaic cells were performed on a CEP-2000 integrated system manufactured by Bunkoukeiki Co. The integration of EQE data over a AM 1.5G solar spectrum yielded calculated J_{sc} values with an experimental variation of less than 10% was relative to the J_{sc} measured under 100 mW cm^{-2} simulated AM 1.5G light illumination.

Electron-only devices were fabricated with the structures of ITO/ZnO (20 nm)/USQ:PC$_{71}$BM (1:3, wt%, 65 nm)/BCP (6, 10 or 14 nm)/Al (100 nm). We measured the dark current density-

voltage characteristics of these devices and then fitted the results using the space charge limited current (SCLC) model.[8, 9] The current density (J) is given by

$$J = \frac{9}{8}\varepsilon_0\varepsilon_r\mu\frac{V^2}{L^3}$$

(3)

Where ε_0 is the permittivity of free-space, ε_r is the relative dielectric constant of the active layer, μ is the charge carrier mobility, and L is the thickness of the active layers.

Samples for atomic force microscopy (AFM) measurements were prepared by spin-casting from USQ:PC$_{71}$BM (1:3, wt%) chloroform solution with a total concentration of 20 mg mL^{-1} (3500 rpm, 45 s) on glass substrates.

The transmission electron microscopy (TEM) investigation was performed on a JEM-2100F field emission transmission electron microscope. The PEDOT:PSS layer was prepared by spin casting their water solution on the glass substrate (3000 rpm, 40 s) and then baked at 150°C for 10 min. The specimen for TEM measurement was prepared by spin-casting the blend chloroform solution (USQ:PC$_{71}$BM = 1:3, wt% 20 mg mL^{-1}) on the PEDOT:PSS substrate, then floating the film on water surface, and transferring to copper grids.

1.6. Synthesis

The synthetic routes of intermediates and target molecules are outlined in **Scheme S1**. Compounds **BIISQ**, **1-4** were prepared according to the procedures described in the literatures.[4, 10-12] All the chemicals, reagents, and solvents were used as received from the suppliers unless otherwise noted.
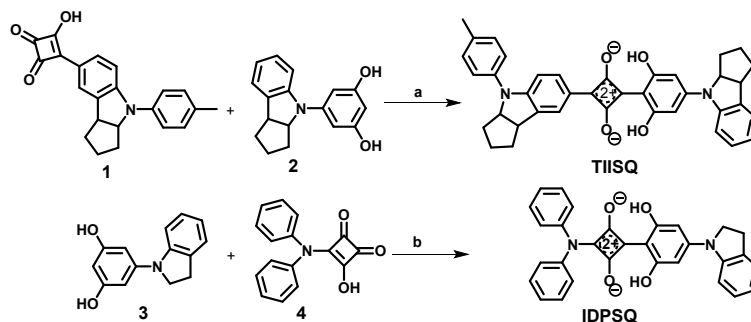
Scheme S1. Synthetic routes of **TIISQ** and **IDPSQ**. (a) *n*-butanol/toluene = 1:3 (v/v), 140° C under Ar, 24 h, 54%; (b) *n*-butanol/toluene = 1:3 (v/v), 140° C under Ar, 14 h, 28%.

2-(2,6-dihydroxy-4-(1,2,3,3a-tetrahydrocyclopenta[*b*]indol-4(8*b*H)-yl)phenyl)-4-(4-*p*-tolyl-1,2,3,3a,4,8b-hexahydrocyclopenta[*b*]indol-7-yl)cyclobuta-1,3-diene-1,3-bis(olate) (TIISQ)   A mixture of compound **1** (345 mg, 1.16 mmol) and **2** (267 mg, 1.16 mmol) in *n*-butanol (7 mL) and toluene (21 mL) was heated at 140° C under Ar for 24 h. Then the reaction mixture was concentrated in vacuo, and the crude product was purified by column chromatography (hexane/dichloromethane = 1/2, v/v) and followed by recrystallization from dichloromethane/hexane and dichloromethane/methanol to give green shiny crystals of **TIISQ** (370 mg, 54%). m.p. 234-236° C. FT-IR: v = 1637 cm^{-1}. ^{1}H NMR (400 MHz, CDCl$_3$, ppm) δ 12.67 (br, 2H, OH), 8.02 (dd, J = 8.8, 1.6 Hz, 1H, ArH), 7.98 (t, J = 1.2 Hz, 1H, ArH), 7.41 (d, J = 8.4 Hz, 1H, ArH), 7.25 (d, J = 8.8 Hz, 2H, ArH), 7.21-7.18 (m, 4H, ArH), 7.02 (t, J = 7.2 Hz, 1H, ArH), 6.74 (d, J = 8.8 Hz, 1H, ArH), 6.33 (s, 2H, ArH), 4.97 (t, J = 6.4 Hz, 1H, CH), 4.71 (td, J = 8.0, 3.2 Hz, 1H, CH), 3.93 (t, J = 8.0 Hz, 1H, CH), 3.86 (t, J = 8.4 Hz, 1H, CH), 2.39 (s, 3H, CH$_3$), 2.15-2.01 (m, 3H, CH$_2$), 1.97-1.92 (m, 3H, CH$_2$), 1.88-1.84 (m, 1H, CH$_2$), 1.76-1.64 (m, 3H, CH$_2$), 1.56-1.33 (m, 2H, CH$_2$). ^{13}C NMR (100 MHz, CDCl$_3$, ppm) δ 182.9, 177.9, 166.1, 164.7, 155.4, 154.6, 143.1, 137.6, 136.9, 136.8, 135.8, 133.1, 130.4, 127.6, 126.2, 125.0, 123.8, 123.2, 120.6, 115.0, 108.0,

107.9, 96.7, 71.0, 69.0, 45.6, 44.4, 35.4, 34.6, 33.5, 32.8, 24.3, 24.0, 21.1. HRMS (ESI)$^+$ *m/z*: [M+H]$^+$ calcd. for $C_{39}H_{35}N_2O_4$: 595.2591; found: 595.2592. Anal. Calcd for $C_{39}H_{34}N_2O_4$: C, 78.77; H, 5.76; N, 4.71; O, 10.76. Found: C, 78.33; H, 5.85; N, 4.55; O, 11.27.

2-(2,6-dihydroxy-4-(indolin-1-yl)phenyl)-4-(diphenylamino)cyclobuta-1,3-diene-1,3-bis(olate) (IDPSQ)   A mixture of compound **3** (342 mg, 1.51 mmol) and **4** (400 mg, 1.51 mmol) in *n*-butanol (4 mL) and toluene (12 mL) was heated at 140° C under Ar for 14 h. Then the reaction mixture was concentrated in vacuo, and the crude product was purified by column chromatography (hexane/dichloromethane = 1/4, v/v) and followed by recrystallization from dichloromethane/methanol and dichloromethane/hexane to give purple crystals of **IDPSQ** (200 mg, 28%). m.p. 250-251ºC. FT-IR: *v* = 1635 cm^{-1}. ^{1}H NMR (400 MHz, CDCl$_3$, ppm) δ 11.98 (s, 2H, OH), 7.50-7.41 (m, 7H, ArH), 7.29-7.24 (m, 4H, ArH), 7.22 (d, *J* = 6.8 Hz, 1H, ArH), 7.17 (t, *J* = 8.0 Hz, 1H, ArH), 6.94 (t, *J* = 7.6 Hz, 1H, ArH), 6.26 (s, 2H, ArH), 4.05 (t, *J* = 8.0 Hz, 2H, CH), 3.14 (t, *J* = 8.0 Hz, 1H, CH). ^{13}C NMR (100 MHz, CDCl$_3$, ppm) δ 178.3, 175.5, 166.6, 163.7, 154.3, 143.5, 139.7, 133.4, 129.3, 128.6, 127.4, 125.4, 122.6, 113.8, 105.4, 96.3, 52.0, 27.9. HRMS (ESI)$^+$ *m/z*: [M+H]$^+$ calcd. for $C_{30}H_{23}N_2O_4$: 475.1669; found: 475.1664. Anal. Calcd for $C_{30}H_{22}N_2O_4$: C, 75.94; H, 4.67; N, 5.90; O, 13.49. Found: C, 75.07; H, 4.83; N, 5.56; O, 14.54.

Table S1. Summary of crystal data, data collection, and refinement parameters for the three USQs.

Compound	**BIISQ**	**TIISQ**	**IDPSQ**
Empirical formula	$C_{40}H_{38}N_2O_4$	$C_{39}H_{34}N_2O_4$	$C_{30}H_{22}N_2O_4 \cdot 0.5CH_2Cl_2$
Formula weight	610.72	594.68	516. 96

Temperature	140.15 K	143 K	293 K
Crystal system	monoclinic	triclinic	monoclinic
Space group	P2$_1$/n	P1	P2$_1$/n
a/Å	13.6013(7)	10.8776(8)	11.8232(8)
b/Å	15.3860(6)	12.2628(8)	14.4169(9)
c/Å	15.6472(9)	15.8498(8)	14.7764(9)
α/°	90.00	103.335(5)	90
β/°	109.803(4)	105.575(6)	104.264(7)
γ/°	90.00	108.689(6)	90
Volume/Å^3	3080.8(3)	1809.3(2)	2441.1(3)
Z	4	2	4
ρ_{calc}mg/mm^3	1.317	1.092	1.407
m/mm^{-1}	0.673	0.071	0.199
F(000)	1296.0	628.0	1076.0
Crystal size/mm^3	0.08 × 0.04 × 0.03	0.6 × 0.3 × 0.2	/
Radiation	CuKα (λ = 1.5418)	MoKα (λ = 0.7107)	MoKα (λ = 0.7107)
2θ range for data collection	7.462 to 139.114°	5.936 to 58.856°	7.53 to 52.744
Index ranges	-15 ≤ h ≤ 16, -18 ≤ k ≤ 18, -18 ≤ l ≤ 18	-14 ≤ h ≤ 12, -15 ≤ k ≤ 16, -20 ≤ l ≤ 21	-14 ≤ h ≤ 14, -17 ≤ k ≤ 18, -18 ≤ l ≤ 12
Reflections collected	19712	16147	14787
Independent reflections	5575 [R$_{int}$ = 0.1046]	8322 [R$_{int}$ = 0.0252]	4979 [R$_{int}$ = 0.0423]
Data/restraints/parameters	5575/340/498	8322/8/451	4979/0/345
Goodness-of-fit on F^2	1.020	0.954	1.090
Final R indexes [I>=2σ (I)]	R$_1$ = 0.0777, wR$_2$ = 0.2034	R$_1$ = 0.0890, wR$_2$ = 0.2484	R$_1$ = 0.0637, wR$_2$ = 0.1582
Final R indexes [all data]	R_1 = 0.1119, wR_2 = 0.2364	R$_1$ = 0.1694, wR$_2$ = 0.3026	R$_1$ = 0.0798, wR$_2$ = 0.1759
Largest diff. peak/hole / e Å^{-3}	0.30/-0.27	0.28/-0.21	0.81/-1.23

Table S2. Summary of the positive and negative electrostatic potential for the three USQs.

	Surface maxima (kcal mol⁻¹)				Surface minima (kcal mol⁻¹)			
BIISQ	29.38	21.64	18.02	17.35	-37.68	-35.40	-33.38	-32.37
TIISQ	23.80	18.91	17.82	17.57	-37.78	-36.40	-34.23	-32.57
IDPSQ	18.28	18.24	17.67	17.55	-38.63	-38.39	-32.63	-31.27
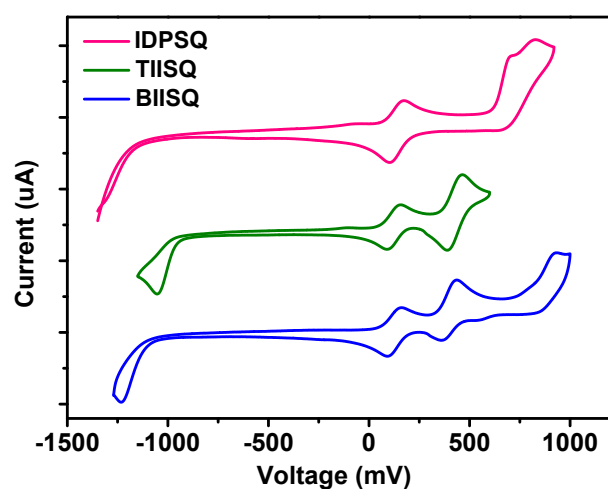
Fig. S1. Cyclic voltammograms of the three USQs in CH₂Cl₂ solution.
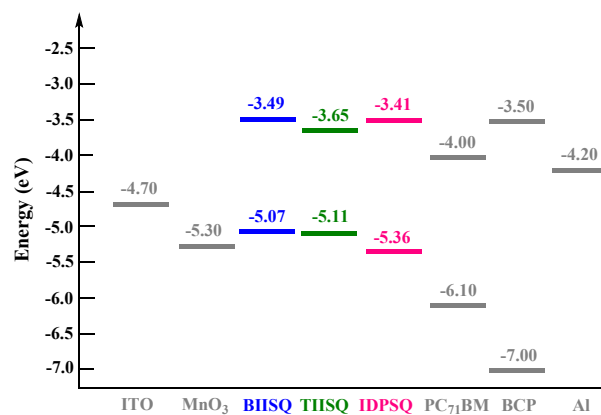
Fig. S2. The energy levels of the components for organic photovoltaic devices.[13, 14]
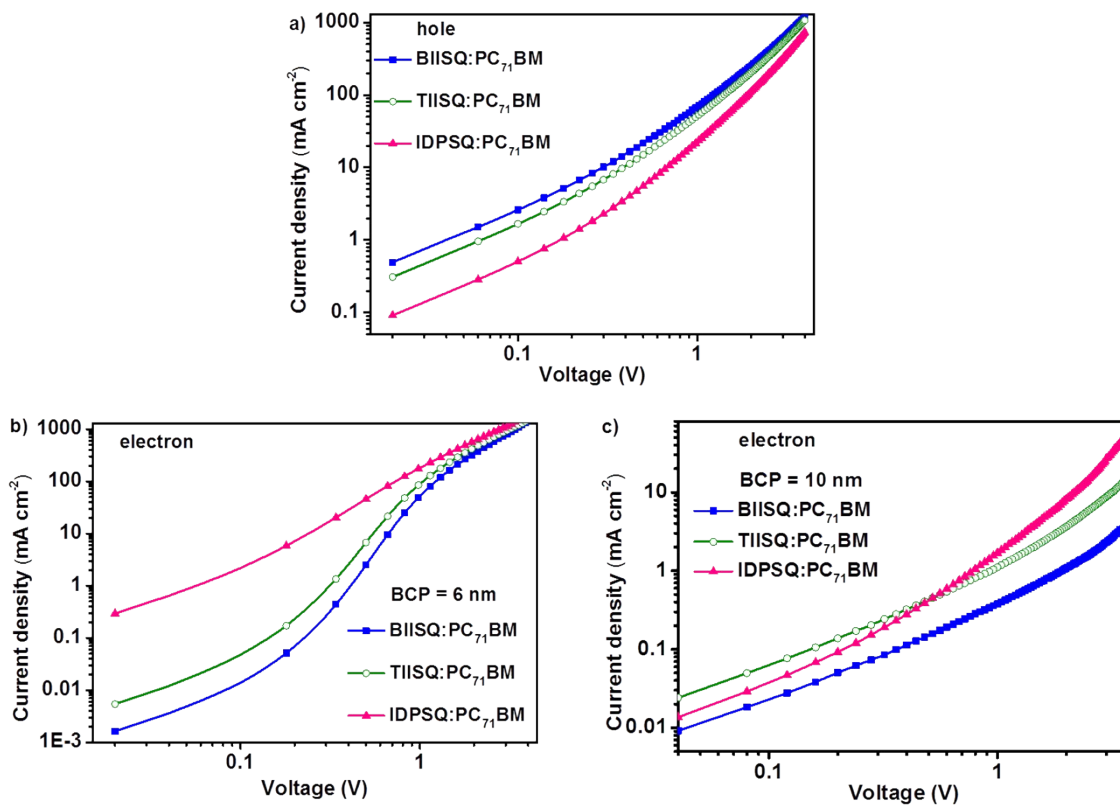
Fig. S3. Current density-voltage characteristics of electron-only single-carrier devices using USQ:PC$_{71}$BM (1:3) blending films as active layers.
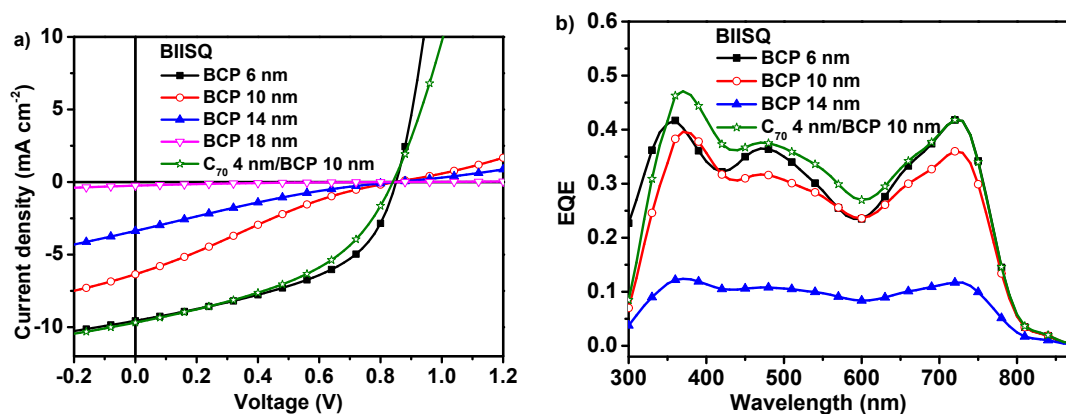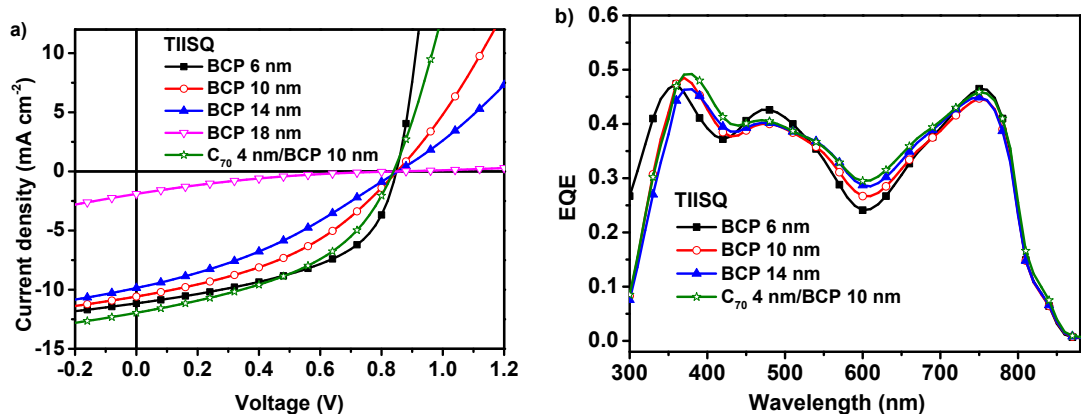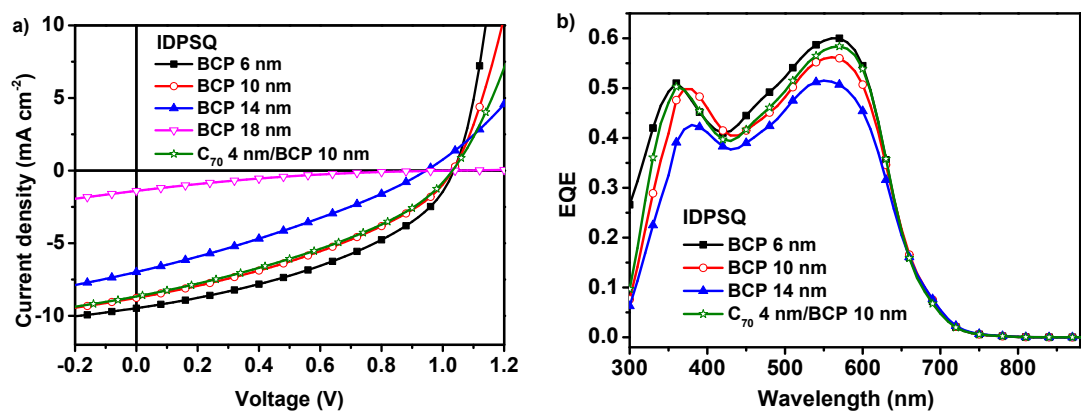

Fig. S4. The *J-V* characteristics under 100 mW cm^{-2} simulated AM 1.5G light illumination (a) and EQE curves (b) of the BHJ-OPV devices based on **BIISQ**:PC$_{71}$BM = 1:3 with different thickness of BCP and C$_{70}$.

Fig. S5. The *J-V* characteristics under 100 mW cm^{-2} simulated AM 1.5G light illumination (a) and

EQE curves (b) of the BHJ-OPV devices based on **TIISQ**:PC$_{71}$BM = 1:3 with different thickness

of BCP and C$_{70}$.

Fig. S6. The *J-V* characteristics under 100 mW cm^{-2} simulated AM 1.5G light illumination (a) and

EQE curves (b) of the BHJ-OPV devices based on **IDPSQ**:PC$_{71}$BM = 1:3 with different thickness
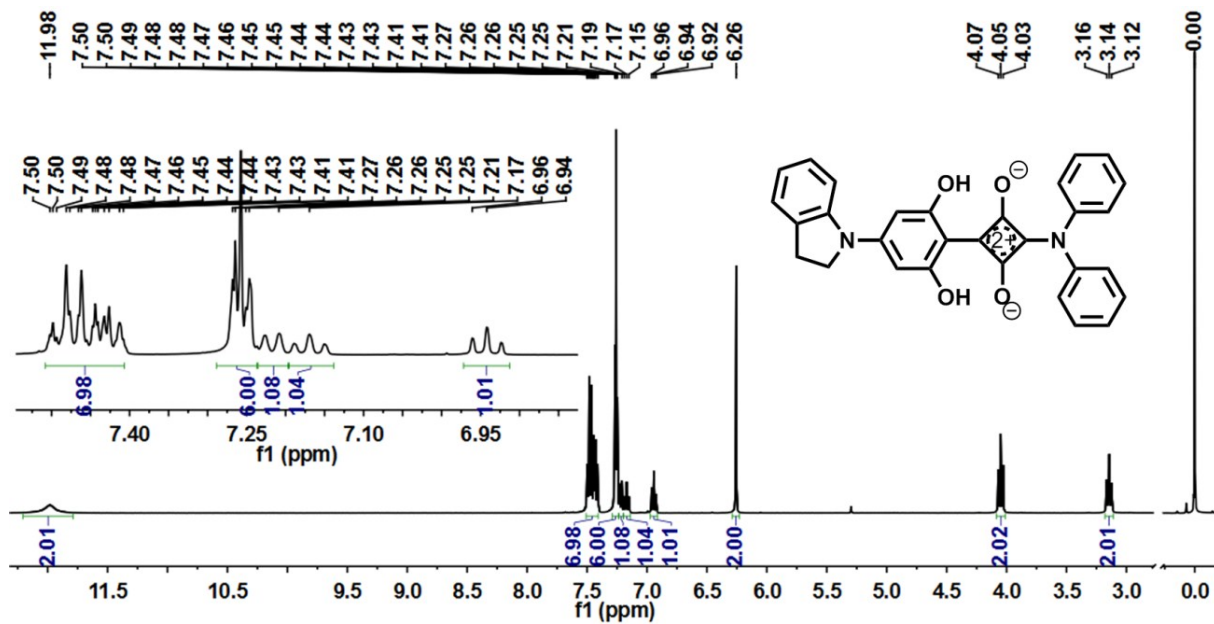
of BCP and C$_{70}$.
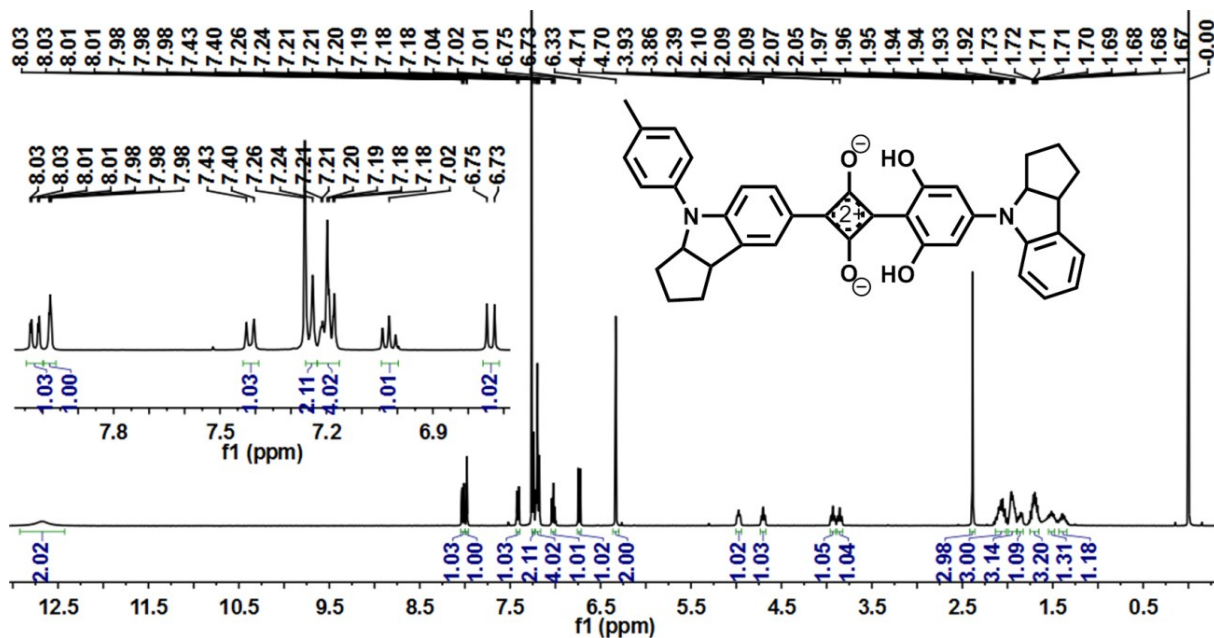
Fig. S7. The ^{1}H NMR spectrum of **TIISQ**.

Fig. S8. The ^{1}H NMR spectrum of **IDPSQ**.
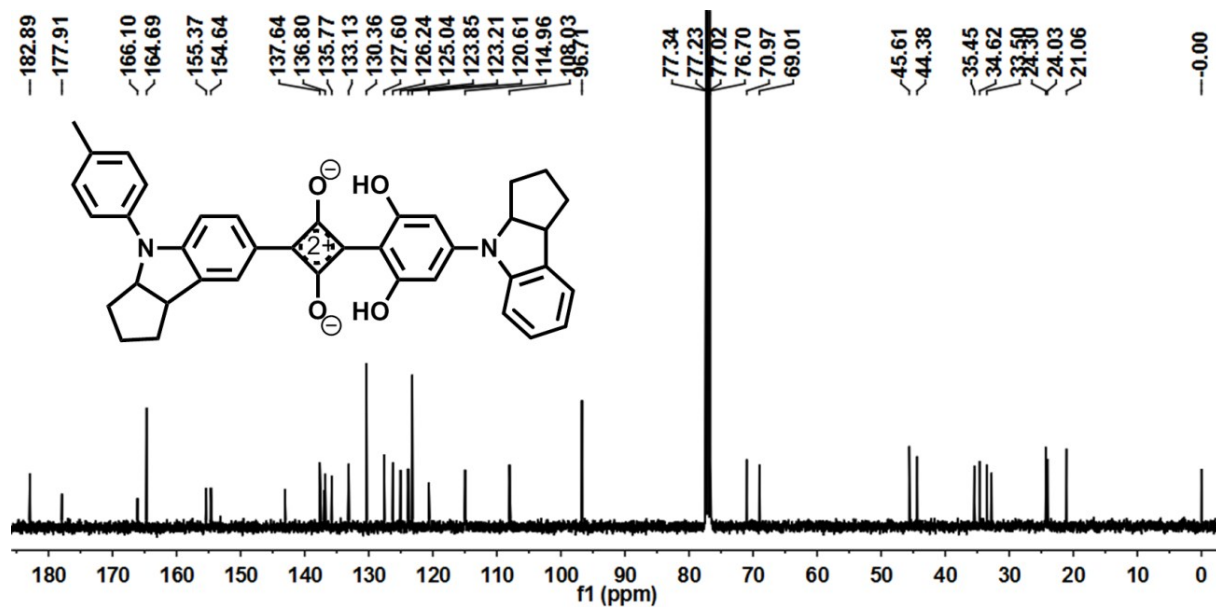
Fig. S9. The ^{13}C NMR spectrum of **TIISQ**.
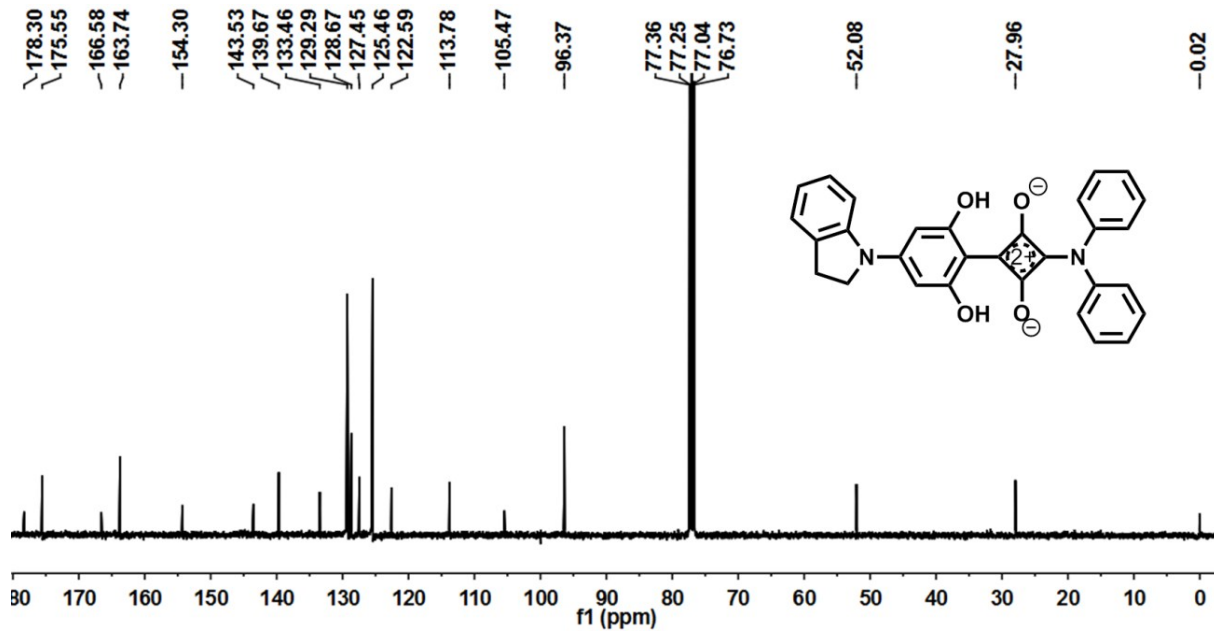

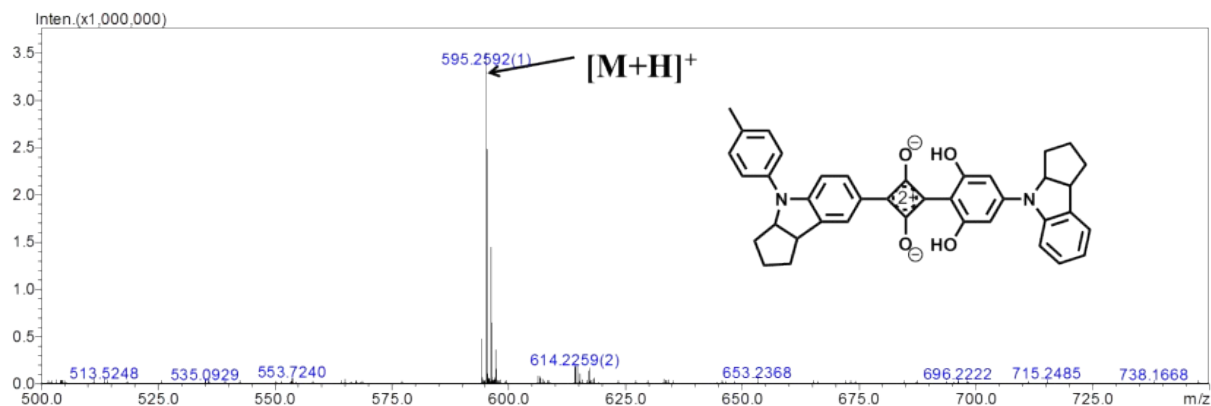**Fig. S10**. The ^{13}C NMR spectrum of **IDPSQ**.

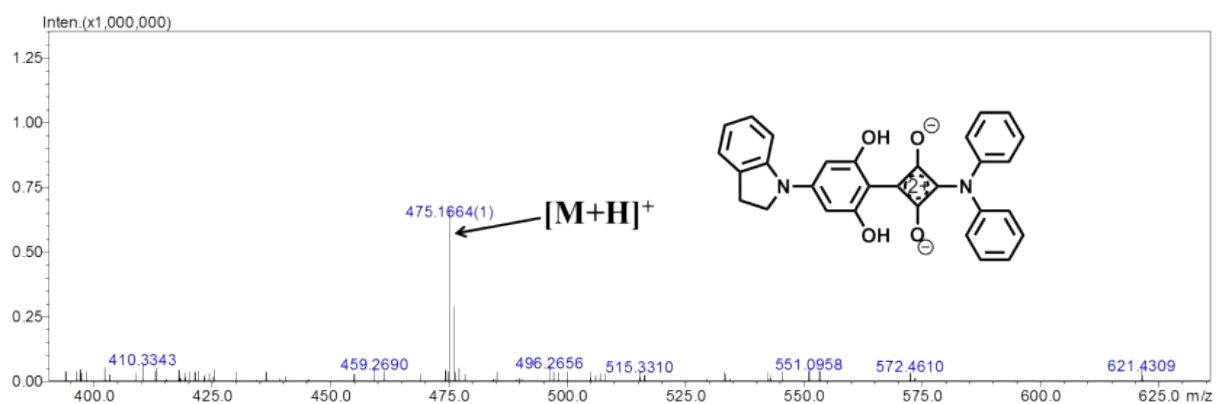**Fig. S11**. The HRMS spectrum of **TIISQ**.

Fig. S12. The HRMS spectrum of **IDPSQ**.

Reference

1   B. Kan, M. Li, Q. Zhang, F. Liu, X. Wan, Y. Wang, W. Ni, G. Long, X. Yang, H. Feng, Y. Zuo, M. Zhang, F. Huang, Y. Cao, T. P. Russell and Y. Chen, *J. Am. Chem. Soc.*, 2015, **137**, 3886-3893.

2   B. Kan, Q. Zhang, M. Li, X. Wan, W. Ni, G. Long, Y. Wang, X. Yang, H. Feng and Y. Chen, *J. Am. Chem. Soc.*, 2014, **136**, 15529-15532.

3   D. Yang, H. Sasabe, J. Yan, T. Zhuang, Y. Huang, X. Pu, T. Sano, Z. Lu and J. Kido, *J. Mater.*

Chem. A, 2016, **4**, 18931-18941.

4   L. Yang, Q. Yang, D. Yang, Q. Luo, Y. Zhu, Y. Huang, S. Zhao and Z. Lu, *J. Mater. Chem. A*, 2014, **2**, 18313-18321.

5   M. J. Frisch, G. W. Trucks and H. B. Schlegel, Gaussian 09; Gaussian, Inc.: Wallingford, CT, 2009.

6   T. Lu and F. Chen, *J. Comp. Chem.* 2012, **33**, 580-592.

7   T. Lu and F. Chen, *J. Mol. Graph. Model.* 2012, **38**, 314-323.

8   H. Azimi, A. Senes, M. C. Scharber, K. Hingerl, C. J. Brabec, *Adv. Energy Mater.* 2011, **1**, 1162-1168.

9   Y. Zhu, L. Yang, S. Zhao, Y. Huang, Z. Xu, Q. Yang, P. Wang, Y. Li, X. Xu, *Phys. Chem. Chem. Phys.* 2015, **17**, 26777-26782.

10 D. Yang, Q. Yang, L. Yang, Q. Luo, Y. Chen, Y. Zhu, Y. Huang, Z. Lu, S. Zhao, *Chem. Commun.* 2014, **50**, 9346-9348.

11 L. Yang, D. Yang, Y. Chen, Q. Luo, M. Zhang, Y. Huang, Z. Lu, H. Sasabe and J. Kido, *RSC Adv.*, 2016, **6**, 1877-1884.

12 S. Wang, L. Hall, V. V. Diev, R. Haiges, G. Wei, X. Xiao, P. I. Djurovich, S. R. Forrest and M. E. Thompson, *Chem. Mater.*, 2011, **23**, 4789-4798.

13 Q. Yang, D. Yang, S. Zhao, Y. Huang, Z. Xu, X. Liu, W. Gong, X. Fan, Q. Huang and X. Xu, *Appl. Surf. Sci.* 2013, **284**, 849-854.

14 G. Chen, H. Sasabe, Z. Wang, X. Wang, Z. Hong, J. Kido and Y. Yang, *Phys. Chem. Chem. Phys.* 2012, **14**, 14661-14666.